IOP Publishing Phys. Scr. 98 (2023) 085311 https://doi.org/10.1088/1402-4896/ace387

Physica Scripta

CrossMark

RECEIVED
23 March 2023

REVISED
18 May 2023

ACCEPTED FOR PUBLICATION
29 June 2023

PUBLISHED
25 July 2023

PAPER

Swift heavy ion irradiation effect on structural, morphological and mechanical properties of $Zr_{70}Ni_{30}$ metallic glass

Wafa Boukhemkhem[1], **Mahmoud Izerrouken**[2], **Matteo Ghidelli**[3], **Thomas Pardoen**[4], **Ali Sari**[5], **Abdel Yazid Khereddine**[6] and **Ali Meftah**[1]

[1] Laboratory of Research on the Physico-Chemistry of Surfaces and Interfaces (LRPCSI), Department of Physics, Faculty of Sciences, University 20 August 1955 Skikda BP 26, 21000 Skikda , Algeria
[2] Nuclear Research Center of Draria, BP 43, Sebbala, Draria, Algiers, Algeria
[3] Laboratoire des Sciences des Procédés et des Matériaux (LSPM), CNRS, Université Sorbonne Paris Nord, 93430, Villetaneuse, France
[4] Institute of Mechanics, Materials and Civil Engineering, UCLouvain, Place Sainte-Barbe 2, 1348 Louvain-la-Neuve, Belgium
[5] Nuclear Research Center of Birine, BP 108, Ain-Oussera, Djelfa, Algeria
[6] Center for Development of Advanced Technologies, (CDTA), 20 août 1956 city, Baba Hassen, BP: 17, DZ-16303, Algiers, Algeria

E-mail: m-izerrouken@crnd.dz

Keywords: $Zr_{70}Ni_{30}$ metallic glass, ion irradiation, structural evolution, thermal spike model

Abstract

Metallic glass films are considered for coating applications in the nuclear field owing to their advantageous performances. However, the response to irradiation remains to be more thoroughly characterized. $Zr_{70}Ni_{30}$ metallic glass films were irradiated by 0.71MeV/u $^{129}Xe^{23+}$ ions in the fluence range from 5×10^{12} to 8×10^{13} ions cm^{-2}. The structural, morphological, and mechanical properties were determined using grazing incidence X-ray diffraction (GI-XRD), atomic force microscopy (AFM), and nanoindentation for the as-deposited and irradiated samples. The Xe ion induced surface smoothening, thereby increasing the corrosion resistance. One-dimensional power spectral density of the AFM data of irradiated film demonstrated that the irradiation-induced evolution of the surface morphology could be attributed to a transition between viscous flow and the evaporation-condensation mechanism. The amorphous structure was unaffected after irradiation up to a fluence of 8×10^{13} ions cm^{-2}. Nanoindentation revealed first a softening as the fluence increases up to 4×10^{13} ions cm^{-2}, reflecting the creation of free volume defects. Then the hardness and Young's modulus slightly increase when reaching 8×10^{13} ions cm^{-2}. Moreover, at a critical dose of 0.008 dpa, the hardness is found to increase. Moreover, the calculation of the inelastic thermal spike model reveals the formation of the track with a radius of 7 nm.

1. Introduction

Zirconium alloys constitute one of the most attractive and convenient materials for cladding applications in nuclear reactors owing to the low thermal neutron capture cross-section and adequate mechanical performances [1, 2]. In contrast to the conventional crystalline Zr-alloys, amorphous alloys or metallic glasses (MGs) counterparts with diverse compositions were processed through exploiting their high glass-forming ability [3, 4]. MGs show a liquid-like atomic configuration and the absence of crystalline defects such as grain boundaries and dislocations [5, 6]. This confers interesting mechanical and chemical properties such as high strength (2-3 GPa), high elastic limit (2 %), good fracture toughness (40-50 MPa m$^{-1/2}$), and excellent resistance to corrosion [4, 6]. Thin-film metallic glasses (TFMGs) can be prepared using different kinds of methods, such as physical vapor deposition (PVD), including evaporation and sputtering [7, 8] and pulsed laser deposition [9], showing fascinating mechanical size effects boosting mechanical properties beyond those of bulk counterparts [10]. For instance, Jiang *et al* [11] found a high elastic strain limit of about 6.6% for the $Ni_{60}Nb_{40}$ metallic glass films. Jang *et al* [12] also observed that the 100 nm Zr-based MG exhibits outstanding combination of high strength (~2.25 GPa) and enhanced ductility (~25%).

In addition, Zr-based MGs have very high thermal stability with an exceptionally wide super cooled liquid region [3, 13] enabling large stability of the glass phase. For these reasons, Zr-based MGs appear as a class of promising candidates in nuclear irradiation environments [14, 15] due to the unique combination of large mechanical properties, thermodynamic stability and the absence of crystalline defects providing a high irradiation resistance, unlike their crystalline counterparts [16, 17]. Li *et al* [16] reported that helium irradiation induced more severe peelings on the surface of the crystalline material $Zr_{67}Ni_{33}$ than the $Zr_{47.9}Ti_{0.3}Cu_{39.3}Ni_{3.1}Al_{9.4}$ bulk MG, which shows the formation of tiny bubbles of helium. On the other hand, according to Wang *et al* [17], in the case of 500 keV helium irradiated polycrystalline tungsten (W) at a fluence of 1×10^{18} ions cm^{-2}, the high-stress concentration at bubbles helium precipitated at grain boundaries causes delamination and peeling, whereas no obvious damage was observed in the $Zr_{64}Cu_{17.8}Ni_{10.7}Al_{7.5}$ bulk MG.

Despite these promising results, few and controversial studies still deal with understanding the structural/mechanical evolution of MGs during irradiation through different categories of radiation (charged particles, neutrons and gamma rays). As an example, irradiation by electrons [18–20] and by ions [21, 22] induces the crystallization of Zr-based MGs ribbons as well as bulk systems [15, 23]. Irradiation-induced crystallization was investigated by Nagase *et al* [24], who proposed three mechanisms to explain this phenomenon: the first one is the increase of free energy of the system, which reaches a threshold value due to the formation of radiation defects such as free volume and anti-free volume inside the amorphous solid. The second one is the random formation of a crystalline cluster near the radiation defects due to a reduction of the local strain, while the facilitated atomic diffusion represents the third one due to the damage caused by irradiation promoting crystallization. Other results, in contrast, indicated that Zr bulk MGs remain amorphous under high energy ion irradiation ($E > 1$MeV) [14, 25, 26]. Different studies reported that ion irradiation induces variations of free volume [27, 28], interatomic spacing [15, 29], and some structural relaxation [30] in the Zr-based MGs. The collapse of short-range order (SRO) has been further reported by Qiu *et al* [31] in $Ni_{50}Nb_{10}Zr_{15}Ti_{15}Pt_{7.5}Cu_{2.5}$ MG ribbon irradiated with 3 MeV Au^{2+} ions at a fluence of 1×10^{14} ions cm^{-2}. Moreover, the mechanical properties were modified after ion irradiation [15, 23]. Iqbal *et al* [23] found that hardness and elastic modulus increase by 43% and 25%, respectively in $Zr_{55}Cu_{30}Al_{10}Ni_5$ amorphous alloy irradiated by 10keV Ar^+. Similar results were also reported by Luo *et al* [15] for $Zr_{61.5}Cu_{21.5}Fe_5Al_{12}$ bulk MG irradiated by 300 keVAr^+ ions due to the precipitation of nanoparticles with a face-centered cubic (fcc) structure and a size of 5nm.

In this paper, we investigate the ion irradiation damage of Zr-Ni thin-film metallic glass. This composition was selected owing to the high stability at room temperature together with a large region of amorphization, from 10 up to 80 at % of Zr [32, 33]. The atomic structure of Zr-Ni metallic glass was investigated in the previous study [34], concluding that the icosahedral clusters are the unit structure of such materials; only a few works have been devoted to radiation damage study in binary Zr-based MGs (Zr-Ni) thin films. The latter studies investigated electrons [19, 20] and 100 keV He ions [35, 36] induced defects in $Zr_{66.7}Ni_{33.3}$ and $Ni_{33}Zr_{67}$ thin films. To our knowledge, no work has been published about the behavior of binary Zr-based MGs (Zr-Ni) thin films under swift heavy ions irradiation, equivalent to fission fragment ejected with high energy ($>$ 100 MeV). In this study, we investigated 0.71 MeV/u Xe ion effect on the mechanical, morphological, and structural properties of $Zr_{70}Ni_{30}$ thin film metallic glass. Various techniques were utilized to provide a thorough understanding of the micro-structured surface evolution and mechanical behavior under ions irradiation. The ultimate objective is to unravel the underlying mechanisms and to determine the potential application of these materials in high-energy environments as coatings for nuclear reactor components. In addition, inelastic thermal spike [37] calculations are performed to further highlight the impact of electronic energy loss and investigate latent track formation in $Zr_{70}Ni_{30}$ metallic glass.

2. Experimental procedures

Zr_xNi_{100-x}($x = 70$ at.%) thin-film metallic glasses (TFMGs) were prepared by a DC-magnetron sputtering system (Alliance Concept AC 450) on a Si (100) substrate within a clean room of class 1,000 to minimize contamination of the sample. The films were deposited at the Plateforme Technologique Amont (PTA) within the Centre Energie Atomique (CEA) in Grenoble. The designed target used for sputtering consisted of rectangular slices made of high-purity Ni (>99.995%) inserted into a Zr matrix of high purity (>99.95%). A fixed distance between the target and substrate at 7 cm was imposed to ensure thickness uniformity. During the experiment, the DC power and the background gas (Ar) pressure remained constant at specific values of 300 W and 0.3 Pa, respectively [10, 38].

After processing, the $Zr_{70}Ni_{30}$ films were irradiated with 0.71MeV/u $^{129}Xe^{23+}$ ions at room temperature to fluences of 5×10^{12}, 1×10^{13}, 2×10^{13}, 4×10^{13} and 8×10^{13} ions cm^{-2}. The irradiations were performed at GANIL, Caen, France, using the IRRSUD beam line. The samples were partially masked, enabling a direct comparison between the irradiated and the non-irradiated parts for each sample. The electronic stopping power S_e, nuclear stopping power S_n and projected ion range R_p deduced using the code SRIM 2008 (Stopping and Range of Ions in Matter) [39] are respectively equal to 23.29 keV nm^{-1}, 0.22 keV nm^{-1} and 7180 nm. The ion range is larger than the film thickness; hence no Xe ion is implanted in the irradiated sample. The displacement per atom (dpa) corresponding to the irradiation fluences was calculated using equation to characterize the irradiation damage [40]:

$$dpa = \frac{\phi \ N_d \ A}{\rho \ d \ N_A}, \tag{1}$$

where ϕ is the Xenon ion fluence, N_d is the number of displacements per ion, A is the target material's molecular mass, ρ is the atomic density of $Zr_{70}Ni_{30}$, d is the penetration depth, and N_A is Avogadro's number. The displacement damage (N_d/d) was calculated using SRIM 2008 code with displacement energy of 40eV for Zr and Ni atoms, respectively [29], and using the 'quick calculation of damage mode.' The total vacancy induced in the layer is 1454 ions^{-1}, leading to a total dose of 0.001, 0.002, 0.004, 0.008 and 0.017 dpa, respectively, for each fluence.

The radiation damage was then investigated using several techniques. The structural characterization was performed by grazing incidence X-ray diffraction (GI-XRD) using a Panalytical X'PERT-PRO MPD X-ray diffractometer with a CuKα_1 radiation ($\lambda = 1.5406$ Å) and a PIXcel 1D detector. The incident angle was optimized to be 1.6° to avoid the influence of the Si substrate on the collected data. The root mean square (RMS) roughness and surface topography of unirradiated and irradiated films were examined using atomic force microscopy (AFM) (type: MFP-3D from Asylum Research, an Oxford Instruments company) in contact mode, with a silicon probe of 9nm tip radius. In addition, the power spectral density (PSD) was then used to provide further information regarding the dominant mechanism responsible for RMS evolution versus fluence. The power spectral density of a surface is a mathematical tool used to decompose the surface into its constituent spatial frequencies (wave vectors) via Fourier analysis of the surface [41]. The one-dimensional PSD is calculated from the AFM images by the WSxM (Windows Scanning X Microscope) software [42].

Nanoindentation experiments were used to probe the mechanical properties. All measurements were carried out using a continuous stiffness measurement (CSM) mode with a Berkovich diamond indenter at room temperature. A maximum load of 3.5 mN and a loading time of 10s were applied for each sample. In order to obtain accurate statistical data, different indents were performed on each sample with 0.15mm spacing between each indent. The hardness (H) and Young's modulus (E) values were determined using the Oliver-Pharr method [43]. Additional analysis using a thermal spike model was also performed to check the effect of 0.71 MeV/u Xe ion irradiation on the formation of the ion track in $Zr_{70}Ni_{30}$.

3. Results and discussion

3.1. Characterization of the as-deposited $Zr_{70}Ni_{30}$ metallic glass

Figure 1(a) shows the GI-XRD spectrum collected in the 2θ range of 20–80°. A broad halo is observed at 37°, confirming the amorphous structure of the $Zr_{70}Ni_{30}$ TFMG, which is according to that finding in previous works [38, 44]. Figure 1(b) shows 2D and 3D AFM images over a 10 μm × 10 μm of the $Zr_{70}Ni_{30}$ film, respectively. The RMS roughness of the surface is about 0.94 ± 0.18 nm and is rather consistent, with little hills (protrusions)-like morphology as indicated by white arrows

Figure 1(c) shows the morphologies of the $Zr_{70}Ni_{30}$ TFMGs in a cross-section view. Observations have been carried out using a field-emission scanning electron microscope (FE-SEM) after cleavage of the Si substrate enabling propagation of a crack from the Si substrate to the films, see [45, 46] for more details, figure 1 (c) reveals that the film thickness is uniform, with a variation of only a few nm, as expected for sputter deposition [45]. The film thickness is about 1200 nm. The hardness (H) and Young's modulus (E) are respectively equal to 7.7 ± 0.45 GPa and 105.8 ± 11.3 GPa, similar to the values determined by Volland *et al* [47].

3.2. Irradiation effects on the $Zr_{70}Ni_{30}$ metallic glass properties

3.2.1. Structural evolution

The The GI-XRD patterns obtained before and after irradiation are provided in figure 2. All patterns show a broad band without any sharp diffraction peaks. This indicates that ion irradiation up to a fluence of 8×10^{13} ions cm^{-2} does not modify the structure of $Zr_{70}Ni_{30}$ TFMG, and that all samples are still amorphous. The maintained amorphous structure is in agreement with the results obtained on $Zr_{67}Ni_{33}$ MG irradiated by 100 keV He ion at a fluence lower than 6×10^{17} He cm^{-2} [35, 36]. On the other hand, the electron irradiation-induced crystallization was reported in the works conducted by Nagase *et al* [19, 20] on $Zr_{66.7}Ni_{33.3}$ amorphous alloy irradiated at room temperature with 2 MeV electrons for a flux between 1.6×10^{24} and 1.1×10^{25}m^{-2} s^{-1}.

However, after fitting the results with a Lorentzian function, no clear evolution of the band position and of the full width at half maximum (FWHM) of the band after ion irradiation was found in the investigated fluence range from 5×10^{12} to 8×10^{13} ions cm^{-2}. In the literature, contradictory results show the band position

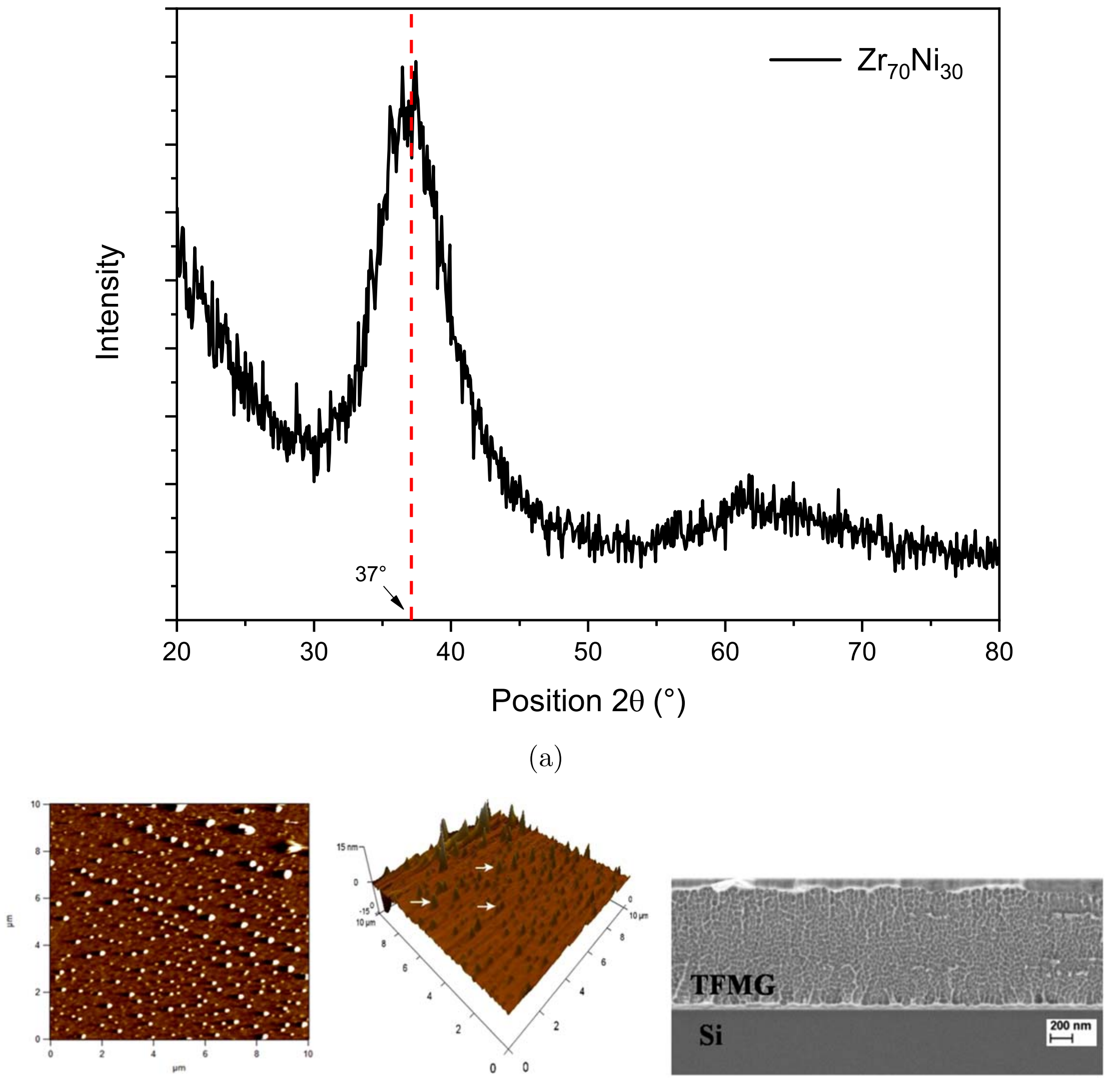

Figure 1. (a) Grazing incidence X-ray diffraction (GI-XRD) pattern in the range of 20–80°. Dashed line shows the center of the broad halo at 37°, (b) Two—and three—dimensional AFM images and (c) Cross-sectional FE-SEM micrograph of the as-deposited $Zr_{70}Ni_{30}$ thin-film metallic glass.

shifting or remaining unchanged without any form of precipitation of crystals. For example, for $Zr_{50.7}Cu_{28}Ni_9Al_{12.3}$ MG irradiated with 7 MeV Xe^{26+} ions in the dose range (0.5 and 1 dpa), Bian *et al* [28] found band position shifts towards a lower angle after irradiation, interpreted as an increase of the average inter-atomic spacing associated with an increase of free volume. Qiu *et al* [31] found that for $Ni_{50}Nb_{10}Zr_{15}Ti_{15}Pt_{7.5}Cu_{2.5}$ MG ribbon irradiated by 3 MeV Au^{2+}, no apparent change in the broad peak position, they also reported that at a low dose of 0.49 and 4.9 dpa, the destruction of the short-range order (SRO) was occurred, which leads to an excess of free volume, with a further increase of the dose to 49 dpa, the free volume decreases which is attributed to the formation of a local structure caused by the enhancement of atomic mobility.

3.2.2. Surface morphology evolution

The The surface morphology after $0.71 MeV/u$ $^{129}Xe^{23+}$ ion irradiation at different fluences is shown in figure 3.

The small hills observed on the deposited sample disappear after ion irradiation, and the surface becomes smoother. This is further confirmed in figure 4, with the root mean square (RMS) roughness evolution under different fluences. First, the RMS roughness decreases in the fluence range of 0 up to 1×10^{13} ions cm^{-2} from 0.94 ± 0.18 nm for unirradiated sample down to 0.19 ± 0.01 nm for sample irradiated at 1×10^{13} ions cm^{-2}. Then, the RMS roughness increases slightly to 0.37 ± 0.09 nm and 0.51 ± 0.02 nm, respectively, at a fluence of 2×10^{13} ions cm^{-2} and 4×10^{13} ions cm^{-2}. Finally, it remains approximately constant at higher fluence, up to 8×10^{13} ions cm^{-2}. The smoothening behavior makes $Zr_{70}Ni_{30}$ a suitable protective coating in nuclear applications since the decrease in roughness increases the corrosion resistance [48–50]. According to the

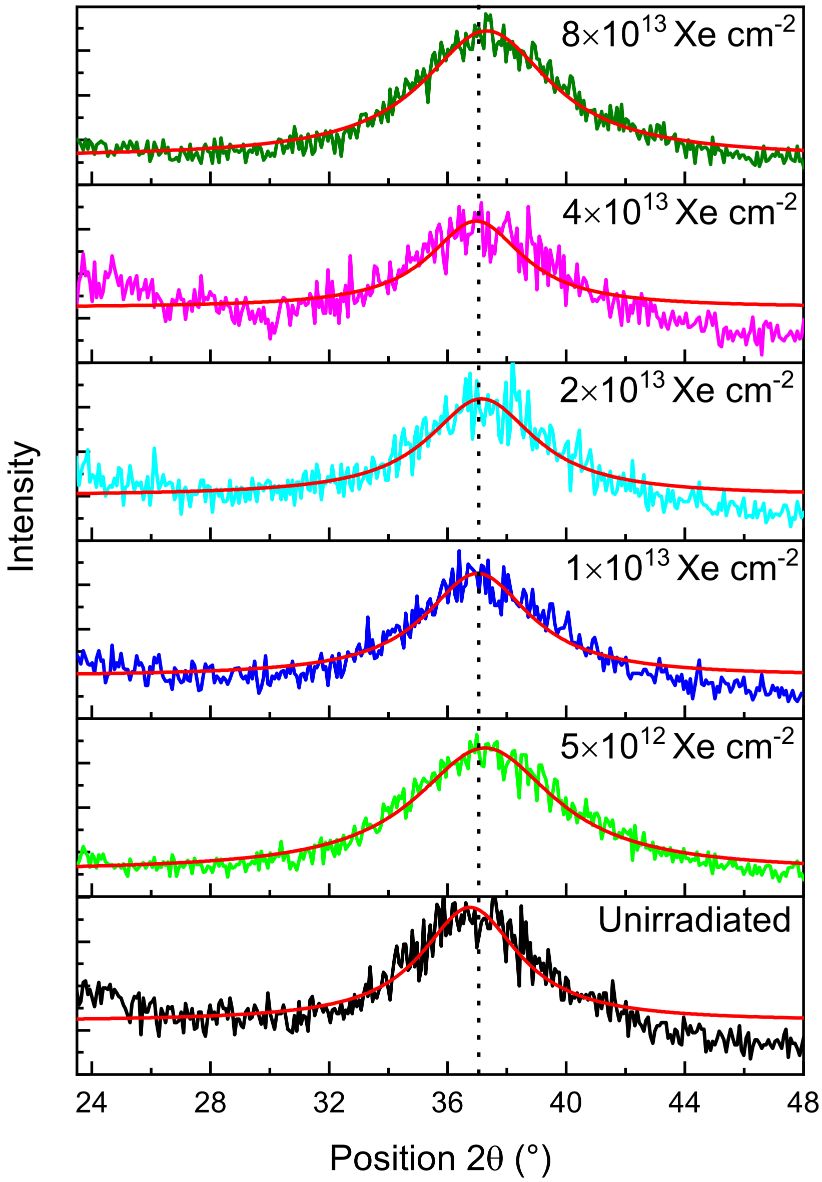

Figure 2. Grazing incidence X-ray diffraction (GI-XRD) patterns of metallic glass $Zr_{70}Ni_{30}$ before and after 0.71MeV/u $^{129}Xe^{23+}$ ion irradiation at different fluences. The vertical dotted line indicates the band position. The red line is the Lorentzian fit of the experimental data.

literature, ion irradiation has thus two main effects on the surface morphology of a solid: surface roughening and smoothening. The first is caused by the sputtering atoms, and the second is induced by material transport [51]. The above results agree with previous work [52] on amorphous Fe-Ni thin films irradiated with 103 MeV Au^{9+} ions. Several authors also reported that irradiation-induced smoothening and roughening phenomena depend on the material, particle energy, and fluence. For example, similar surface smoothening was reported in [53, 54]. Moreover, surface roughening was found in other investigations [55, 56] and attributed to the damage induced under ion irradiation in different metallic glasses.

The power spectral density (PSD) is used to interpret the RMS evolution with irradiation fluence. This gives a representation of the surface roughness amplitude as a function of the spatial frequency of the roughness [41], which helps understand the mechanism responsible for smoothening and roughening of the surface after ion irradiation. The PSD data (see figure 5) show two distinct domains. One domain at a low spatial frequency (region I) corresponds to the uncorrelated white noise, and the second one at a high frequency (region II) represents surface features that are correlated [52, 57]. Moreover, according to Tong and Williams study [58], at low spatial frequency values, a flat plateau extends out to the critical spatial frequency, after which the power spectral density decreases linearly due to surface smoothening. Four mechanisms were discussed; plastic flow, evaporation-condensation, bulk diffusion, and surface diffusion corresponding respectively to the slope values equal to 1, 2, 3 and 4 [59]. In our case, the fitting is performed in the second region, which begins from the critical spatial frequency value (0.045 nm^{-1}).

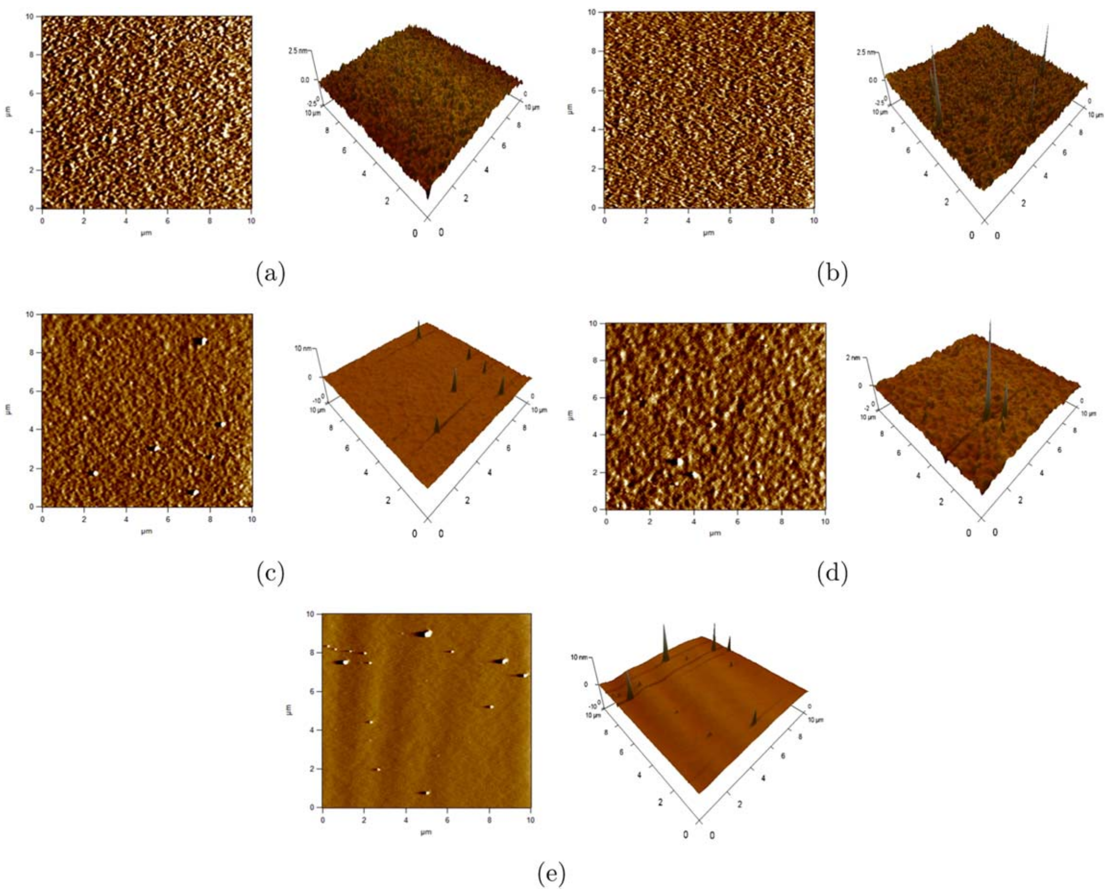

Figure 3. Two-and three-dimensional AFM images of irradiated $Zr_{70}Ni_{30}$ metallic glass at a fluence of (a) 5×10^{12} Xe cm^{-2}, (b) 1×10^{13} Xe cm^{-2}, (c) 2×10^{13} Xe cm^{-2}, (d) 4×10^{13} Xe cm^{-2} and (e) 8×10^{13} Xe cm^{-2}.

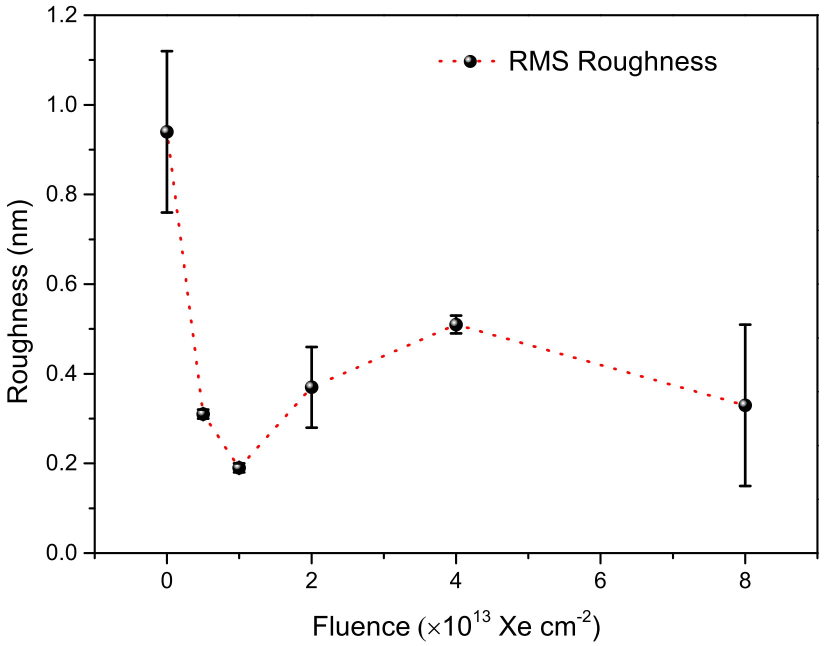

Figure 4. Variation of the roughness as a function of the fluence irradiation for $Zr_{70}Ni_{30}$. The dotted line is to guide the eye. The error bars for RMS represent standard deviations obtained from various experimental measurements.

The slopes of the linear fit are summarized in table 1. When the fluence increases from 0 to 2×10^{13} ions cm^{-2}, the slope varies from 3 to 1. Thus, the surface morphology modification is interpreted as a combination between plastic flow and evaporation-condensation at low fluence ($\leqslant 2 \times 10^{13}$ ions cm^{-2}). At higher fluence

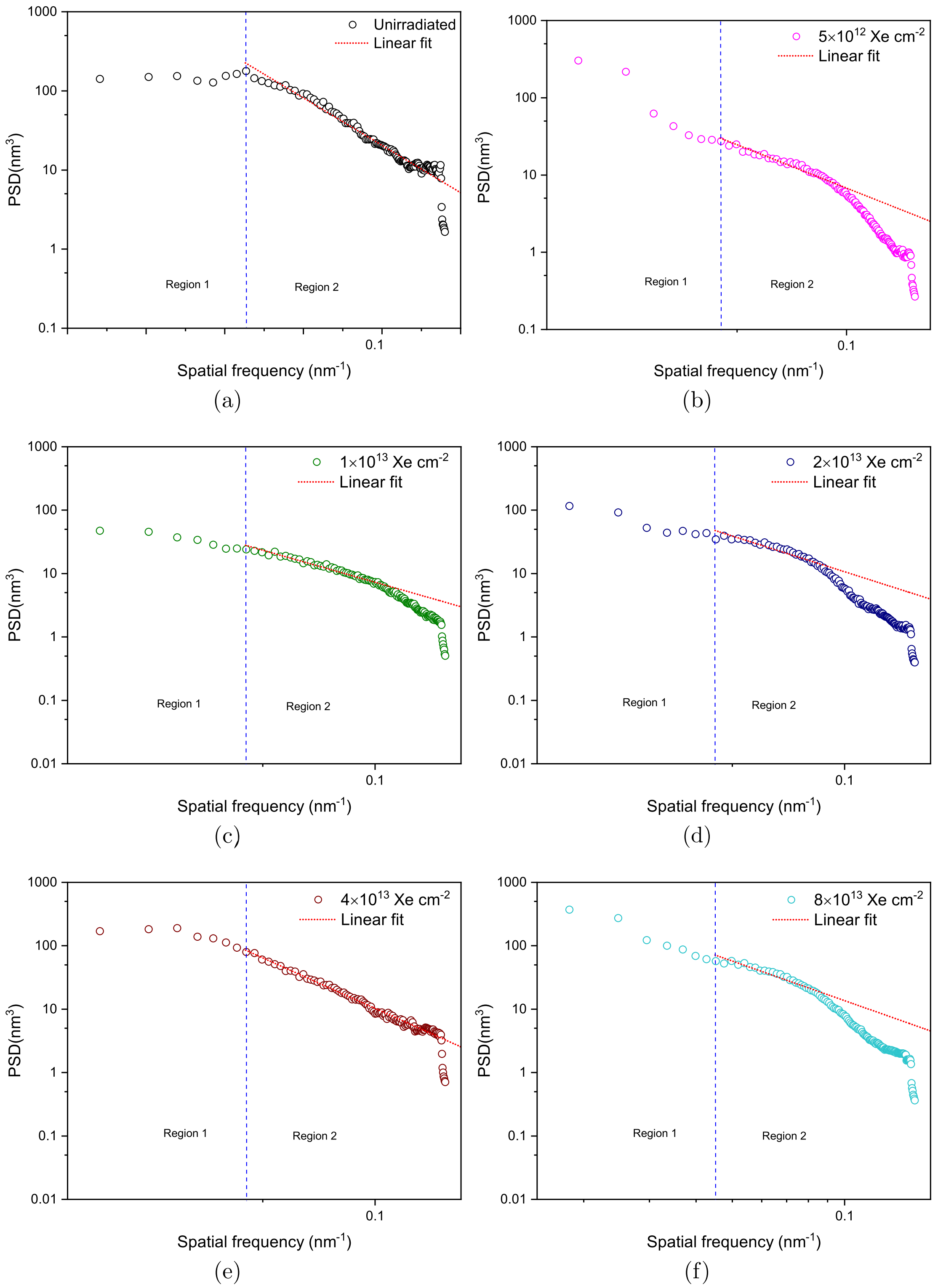

Figure 5. Variation of the power spectral density (PSD) as a function of the spatial frequency of surfaces for $Zr_{70}Ni_{30}$; (a) Unirradiated, and irradiated at different fluences of (b) 5×10^{12} Xe cm^{-2}, (c) 1×10^{13} Xe cm^{-2}, (d) 2×10^{13} Xe cm^{-2}, (e) 4×10^{13} Xe cm^{-2} and (f) 8×10^{13} Xe cm^{-2}. The short red dotted line in the plots denotes the linear fit of the data.

($>2 \times 10^{13}$ ions cm^{-2}), the value is close to 2, which means that the evaporation-condensation process can explain the roughness increase at high fluence. The latter evolution is attributed to the temperature increase along the ion path as found using the thermal spike model addressed hereafter. A similar change of the roughness has been observed by Pookat *et al* [60] in amorphous $Co_{77}Fe_{23}$ thin films irradiated with 100 MeV Ag^{7+}, where the smoothening of the surface topography is due to the viscous flow [61] occurs at a fluence of 2×1^{11} ions cm^{-2} and the evaporation-condensation mechanism caused by the sputtering is already activated at a fluence of 1×10^{12} ions cm^{-2} and 3×10^{13} ions cm^{-2}.

Table 1. Root mean square (RMS) roughness and calculated values of the slope of the power spectral density (PSD) curves of unirradiated and irradiated $Zr_{70}Ni_{30}$ thin film at different fluences.

Irradiation fluence (Xe cm^{-2})	RMS (nm)	Slope of the PSD curves
0	0.94 ± 0.18	2.84 ± 0.04
5×10^{12}	0.31 ± 0.01	1.86 ± 0.06
1×10^{13}	0.19 ± 0.01	1.67 ± 0.03
2×10^{13}	0.37 ± 0.09	1.87 ± 0.10
4×10^{13}	0.51 ± 0.02	2.64 ± 0.04
8×10^{13}	0.33 ± 0.18	2.07 ± 0.09

Table 2. Mechanical properties of the $Zr_{70}Ni_{30}$ thin film before and after ion irradiation from the nanoindentation experiments.

Irradiation fluence (Xe cm^{-2})	Hardness H (GPa)	Young's modulus E (GPa)	H/E
0	7.72 ± 0.45	105.79 ± 11.34	0.07 ± 0.01
5×10^{12}	5.99 ± 0.30	102.35 ± 4.39	0.06 ± 0.01
1×10^{13}	5.55 ± 0.50	88.71 ± 6.86	0.06 ± 0.01
2×10^{13}	5.24 ± 0.60	89.09 ± 9.82	0.06 ± 0.01
4×10^{13}	4.89 ± 0.15	62.63 ± 4.64	0.08 ± 0.01
8×10^{13}	6.00 ± 0.41	81.19 ± 6.10	0.07 ± 0.01

3.2.3. Mechanical properties

The The load-penetration response extracted by nanoindentation were used to determine the mechanical properties reported in table 2.

Figure 6 provides the evolution of hardness (H) and Young's modulus (E) as a function of the fluence. Both (H) and (E) decrease with increasing fluence up to 4×10^{13} ions cm^{-2} from 7.7 ± 0.45 GPa down to 4.9 ± 0.15 GPa and from 105.8 ± 11.3 GPa down to 62.6 ± 4.6 GPa, respectively. This is followed by a slight increase when then fluence grows up to 8×10^{13} ions cm^{-2}.

The Young's modulus of a material is inversely correlated with the distance to neighbor atoms, hence a decrease in the amount of the free volume tends to lead to an increase of the modulus [62]. Thus, the elastic modulus evolution reveals an irradiation-induced free volume enhancement (decrease of atomic density) up to a fluence of 4×10^{13} ions cm^{-2}, which means that the observed reduction in stiffness and strength can be attributed to the damage induced by either free volume or nano-voids through ion-solid collision [63], which probably results in the softening of the $Zr_{70}Ni_{30}$ films. The decrease in stiffness and strength was also observed after ion irradiation at room temperature in several Zr-based bulk metallic glasses [14, 64]. Brechtl *et al* [65] found that fast neutron irradiation ($E_n > 0.1$MeV) at 70 °C to a fluence of 1.4×10^{20} n cm^{-2} induced an excess of free volume defects, which leads to mechanical softening of $Zr_{52.5}Cu_{17.9}Ni_{14.6}Al_{10}Ni_5$ bulk MG and a decrease of Young's modulus. While Onodera *et al* [66] reported that the drop in hardness is attributed to irradiation-induced atomic disordering in the metallic glass. The dose-dependence of the change in hardness in metallic glasses is opposite to what is observed in the case of crystalline pure metals and metallic alloy systems, in which irradiation induces hardening. The evolution of the hardness can be described by the following phenomenological equation [67]:

$$|\Delta H| = |(H - H_0)| = h(dpa)^n, \tag{2}$$

where h and n are two empirical parameters representing the magnitude of irradiation-softening, H_0 is the hardness of an unirradiated sample and H is the hardness after ion irradiation. The variation of $|\Delta H| = |(H - H_0)|$ as a function of the dose (dpa) is given in figure 7 in log-log format. It reveals two distinct irradiation regimes: a low-dose regime and a high-dose regime. In the low-dose regime, n is equal to 0.23. However, the slope changes sign beyond a critical dose of about $D_c = 0.008$ dpa in the high dose-regime. This result reveals that irradiation induces the softening of $Zr_{70}Ni_{30}$ at a dose lower than a critical value of D_c, then the material gradually hardens with increasing dose.

The slight increase of (H) and (E) values at high fluence (8×10^{13} ions cm^{-2}) suggests that the film reached a saturation in the concentration of defects leading to a high atomic mobility, which subsequently favours rearrangement of atomic processes, which can then induce nano-crystals formation due to thermal effects. With

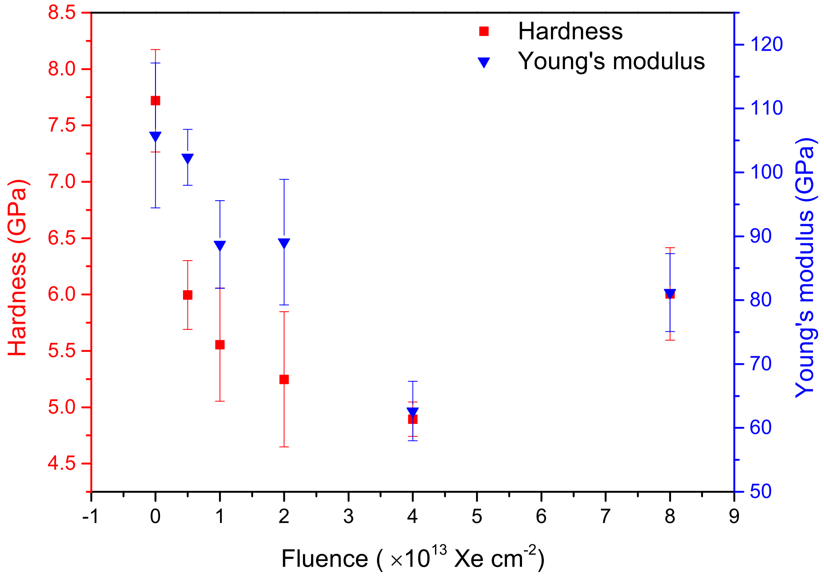

Figure 6. Variation of hardness (H) and Young's modulus (E) of metallic glass $Zr_{70}Ni_{30}$ as a function of fluences irradiation, with the statistical standard deviations obtained from repeated experimental measurements.

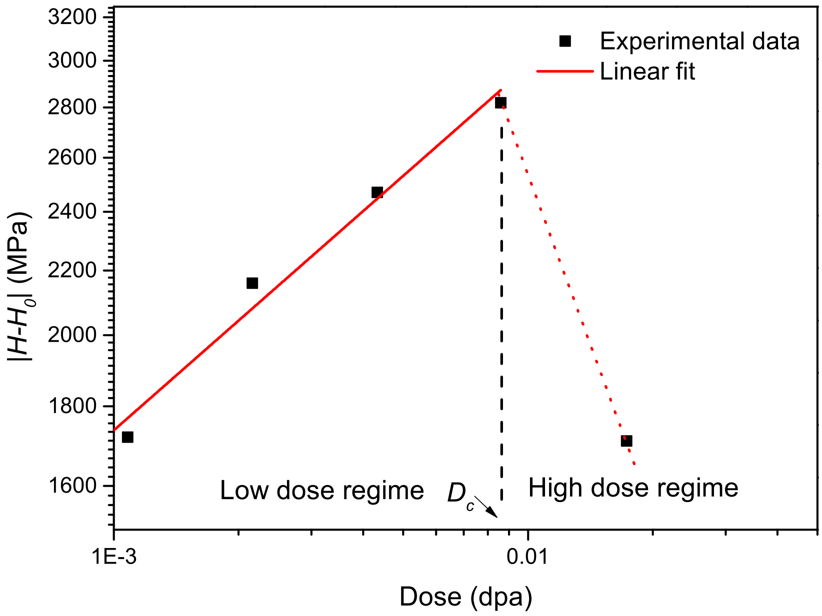

Figure 7. Dose dependence of irradiation softening / hardening in $Zr_{70}Ni_{30}$. The solid line in the plot is the linear fit of the experimental data, while the dotted line represents the dose-dependence in the high dose regime.

a further increase in the irradiation fluence, the amount of free volume is reduced, leading to an increase of hardness [68]. Other studies [15, 69] deduced that the formation of nano-crystals is the fundamental reason for the hardening effect in metallic glasses after ion irradiation. Note that the annealing of Zr bulk MG at 300 °C–325 °C leads to free volume annihilation, resulting in structural relaxation and increased mechanical properties. Indeed, structural relaxation is known to occur through different mechanisms: (i) defects or free volume annihilation; (ii) recombination of defects of opposing character; (iii) change in both topological and compositional short-range order, which can be uncovered through an analysis of the local arrangement of neighboring atoms [70–72]. More research is required to understand the delicate balance of mechanisms that causes the hardness variation at high fluence. In addition, it should also be noted that the irradiated samples exhibit the same evolution of both (H) and (E) parameters as was observed earlier in the case of 7 MeV Xe^{26+} ion irradiated $Zr_{50.7}Cu_{28}Ni_{9}Al_{12.3}$ bulk MG [28], where the mechanical properties tend to decrease for a dose of 1 dpa and then to slightly increase at 5 dpa. Our results suggest a strong correlation between hardness and free volume evolution in agreement also with the previous work by Jiang *et al* [73]. The authors discussed the relationship between the amount of free volume and the mechanical behaviour of metallic glasses.

Finally, table 2 shows also that the H/E ratio, a key parameter in the context of wear resistance [74], slightly decreases after irradiation up to a fluence of 2×10^{13} ions cm^{-2} and then remains almost identical to the unirradiated sample at high fluence ($>2 \times 10^{13}$ ions cm^{-2}). This suggests that ion irradiation does probably not significantly affect the wear resistance of $Zr_{70}Ni_{30}$ metallic glass, which is an interesting finding for application as coating in irradiated environments, especially when exposed to moving fluids, such as coating in the nuclear waste containers [15, 75]. New TFMGs with excellent hardness and corrosion resistance were recently developed (see [76] and references therein), making them attractive for coating structural materials. Due to the limited corrosion of zirconium alloys fuel cladding material under accident conditions, oxidation-resistant coatings are also used to prevent thermal oxidation and consequently protect the zirconium alloy substrate [77, 78]. Therefore, metallic glass coating based on Zr-composition could constitute an attractive option, with expected good adhesion owing to element compatibility.

3.3. Thermal spike model calculations

In order to analyze the swift heavy ion irradiation-induced track formation in amorphous $Zr_{70}Ni_{30}$, the thermal spike model, was applied to take into account only the electronic energy loss S_e (keV Å^{-1}) for $^{129}Xe^{23+}$ ion of a specific energy 0.71MeV/u. According to this model, the heat diffusion in the two; electronic (index e) and atomic (index a) sub-systems is described by the following equations [37]:

$$C_e(T_e)\frac{\partial T_e}{\partial t} = \frac{1}{r}\frac{\partial}{\partial r}\left[rK_e(T_e)\frac{\partial T_e}{\partial r}\right] - g(T_e - T_a) + A(r, t), \quad (3)$$

$$C_a(T_a)\frac{\partial T_a}{\partial t} = \frac{1}{r}\frac{\partial}{\partial r}\left[rK_a(T_a)\frac{\partial T_a}{\partial r}\right] + g(T_e - T_a), \quad (4)$$

where the parameters T_e, T_a, C_e, C_a, K_e and K_a are the temperature, the specific heat capacity and the thermal conductivity of the electronic and atomic subsystems, respectively, g is the electron-phonon coupling, t and r are the variables of the time and space from the ion trajectory, and $A(r, t)$ is the deposited energy to the target electrons obtained from Monte Carlo simulation in the work of Waligórski *et al* [79]. The numerical solution of these two equations gives the temperature evolution for the two subsystems as a function of time (t) and space (r). According to a study conducted by Ichitsubo *et al* [80], the structure of the $Zr_{70}Ni_{30}$ amorphous alloy resembles that of the Zr_2 Ni crystalline phase. So, since there is no literature-available thermodynamic data for $Zr_{70}Ni_{30}$, the calculations were performed using the specific heat of the Zr_2 Ni as a function of the temperature from [81]. The thermal conductivity (K) is estimated using the relationship $K = C\rho$ D where C is the specific heat, ρ is the density, and D=0.02 cm^{2}s^{-1} is the thermal diffusivity [82]. The latent heat of fusion was determined for Zr_2 Ni using the software MTDATA and the SGTE solution database. The value for the coupling parameter used for the simulation was taking from reference [83].

This calculation gives the variation of atomic temperatures in Kelvin as a function of the time and radius of the ion track, as shown in figure 8. The horizontal dotted line indicates the melting temperature (T_m). This plot reveals that the lattice temperature reaches the melting point, indicating the phase solid-liquid transformation. This suggests the melting of $Zr_{70}Ni_{30}$ by swift heavy ion irradiation, leading consequently to track ion formation after the quenching of a melting phase. The track radius is about 7 nm. The track concentration increases with increasing fluence. At high doses these tracks probably accumulate to form nano-crystals responsible for the enhanced mechanical properties of $Zr_{70}Ni_{30}$ metallic glass. In addition, point defects can be induced around the ion track which could decrease the free volume leading to improved mechanical properties (H, E). However, despite the thermal spike process, structural changes within damage cascades coupled with the free volume and anti-free volume have a significant role in forming nano-crystals after irradiation with 1 MeV Ni^+ ion in the $Ni_{25.5}Nb_{10}Zr_{15}Ti_{15}Pt_{7.5}$ metallic glass ribbon [84]. According to the literature, the precipitation of nano-crystals with an average size of 6 nm in the MG under 7MeV Xe^{26+} ion irradiation was found at 5 dpa using the TEM and leading to the increase in the mechanical properties [28]. Hence the amorphous metallic glass $Zr_{70}Ni_{30}$ is therefore sensitive to electronic excitations. Thus, depending on the electronic stopping power, latent tracks with spherical and cylindrical morphology can be induced by irradiation in $Zr_{70}Ni_{30}$ metallic glass, which leads to a change in mechanical, electrical and structural properties.

In order to check the electronic energy loss threshold of track formation in the $Zr_{70}Ni_{30}$ metallic glass under $^{129}Xe^{23+}$ ion irradiation, we carried out a series of calculations starting with the Xe ions energy of 0.71 MeV/u down to a possible low value using the parameters of the thermal spike model described above. Thus, the track radius formed was estimated for each electronic energy loss at different energies. The results given the evolution of the track radius in $Zr_{70}Ni_{30}$ versus electronic energy loss are shown in figure 9. The track radius increases

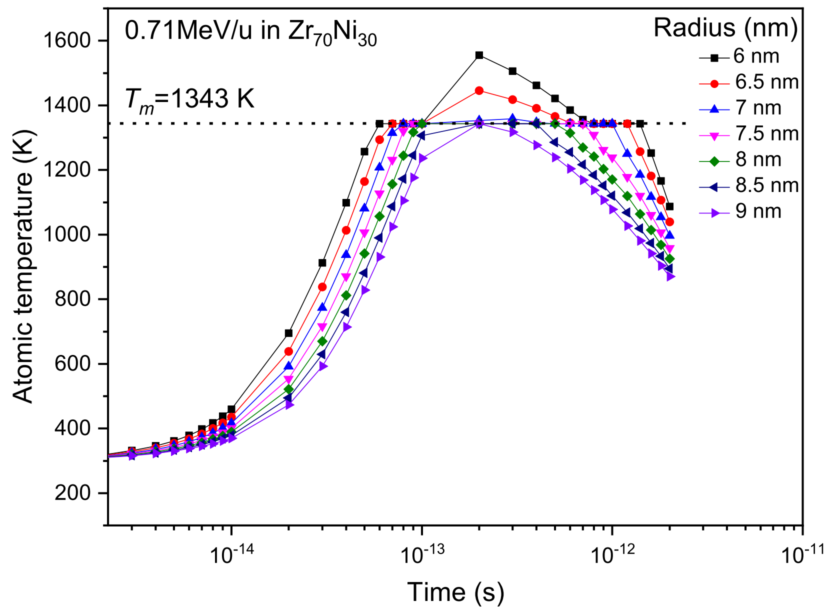

Figure 8. Variation of the atomic temperature for $Zr_{70}Ni_{30}$ as a function of the time at different track radius caused by 0.71MeV/u $^{129}Xe^{23+}$ ions irradiation. The dotted line indicates the melting temperature (T_m).

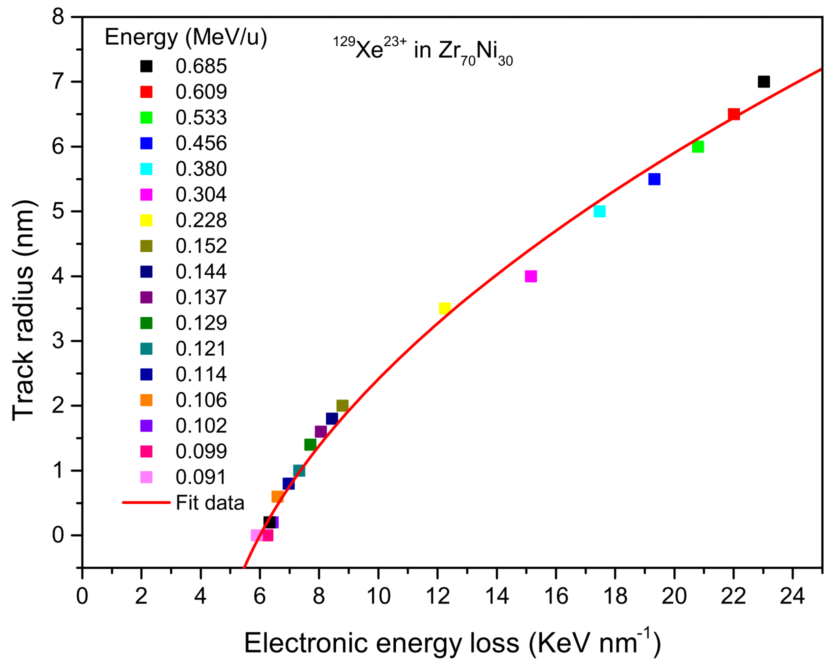

Figure 9. Variation of the track radius as a function of the electronic energy loss in $Zr_{70}Ni_{30}$ thin film for different deposited energies by $^{129}Xe^{23+}$ ion irradiation. The line in the plot is the fit of the data points.

above a threshold value of about 6.32 keV nm^{-1}. Therefore, the track formation radius starts to be observable in the $Zr_{70}Ni_{30}$ at an electronic energy loss threshold of $S_{eth} \geqslant 6.32$ keV nm^{-1}.

4. Conclusion

In this investigation, $Zr_{70}Ni_{30}$ thin film metallic glass deposited onto silicon substrate via the DC magnetron sputtering was irradiated by 0.71MeV/u $^{129}Xe^{23+}$ swift heavy ion within the fluence range from 5×10^{12} to 8×10^{13} ions cm^{-2}. The GI-XRD, SEM and AFM analyses revealed that the films exhibit an amorphous structure with a thickness of about 1200 nm, and the RMS roughness is equal to 0.94 nm. Furthermore, 0.71MeV/u Xe ion irradiation induced surface smoothening, and modification of the hardness and Young's modulus. The combination of the AFM and nano-indentation data reveal that at a low irradiation dose up to a critical value of 0.008 dpa, the irradiation-induced increase of the free volume causes $Zr_{70}Ni_{30}$ softening. A slight increase of the hardness above a dose of 0.008 dpa may be ascribed to nano-crystals formation. This is supported by the results of the thermal spike calculations indicating the formation tracks of 7 nm. Further studies using transmission electron microscopy are needed to confirm the results. This will be the subject of our next work: the evolution of the microstructure under swift heavy ion irradiation.

In addition, the electronic energy loss threshold for track generation in $Zr_{70}Ni_{30}$ was calculated to be 6.32 keV nm^{-1} using thermal spike calculations.

Acknowledgments

This work was supported by the National Fund for Scientific Research (FNRS), under Grant-T.0178.19 for T Pardoen, M Ghidelli. The authors are indebted to GANIL staff for the Xe ions irradiations, Professor Azizi Amor for AFM analysis and Jim A J Robinson, for latent heat of fusion calculation.

Data availability statement

All data that support the findings of this study are included within the article (and any supplementary files).

ORCID iDs

Wafa Boukhemkhem https://orcid.org/0000-0002-0346-3903
Matteo Ghidelli https://orcid.org/0000-0001-6057-9040
Ali Meftah https://orcid.org/0000-0002-9557-3711

References

[1] Hosemann P, Frazer D, Fratoni M, Bolind A and Ashby M 2018 Materials selection for nuclear applications: challenges and opportunities *Scr. Mater.* **143** 181–7
[2] Lemaignan C 2012 Zirconium alloys: properties and characteristics *Comprehensive Nuclear Materials* **2** 217–32
[3] Inoue A 2000 Stabilization of metallic supercooled liquid and bulk amorphous alloys *Acta Mater.* **48** 279–306
[4] Inoue A, Shen B and Nishiyama N 2008 Development and applications of late transition metal bulk metallic glasses *Bulk metallic glasses* (Boston: Springer) 1–25
[5] Basu J and Ranganathan S 2003 Bulk metallic glasses: A new class of engineering materials *Sadhana* **28** 783–98
[6] Ashby M and Greer A L 2006 Metallic glasses as structural materials *Scr. Mater.* **54** 321–6
[7] Lee J, Huang K H, Hsu K C, Tung H C, Lee J W and Duh J G 2015 Applying composition control to improve the mechanical and thermal properties of Zr-Cu-Ni-Al thin film metallic glass by magnetron DC sputtering *Surf. Coat. Technol.* **278** 132–7
[8] Nair B and Priyadarshini B G 2016 Process, structure, property and applications of metallic glasses, AIMS *Mater. Sci.* **3** 1022–53
[9] Almyras G, Matenoglou G, Komninou P, Kosmidis C, Patsalas P and Evangelakis G 2010 On the deposition mechanisms and the formation of glassy Cu-Zr thin films *J. Appl. Phys.* **107** 084313
[10] Ghidelli M, Gravier S, Blandin J J, Djemia P, Mompiou F, Abadias G, Raskin J P and Pardoen T 2015 Extrinsic mechanical size effects in thin ZrNi metallic glass films *Acta Mater.* **90** 232–41
[11] Jiang Q, Liu P, Ma Y, Cao Q, Wang X, Zhang D, Han X, Zhang Z and Jiang J 2012 *Super Elastic Strain Limit in Metallic Glass Films* Scientific report 2 1-6 (https://doi.org/10.1038/srep00852)
[12] Jang D and Greer J R 2010 Transition from a strong-yet-brittle to a stronger-and-ductile state by size reduction of metallic glasses *Nat. Mater.* **9** 215–9
[13] Zhang T, Inoue A and Masumoto T 1991 Amorphous Zr-Al-TM (TM= Co, Ni, Cu) alloys with significant supercooled liquid region of over 100 K *Mater. Trans., JIM* **32** 1005–10
[14] Perez-Bergquist A G, Bei H, Leonard K J, Zhang Y and Zinkle S J 2014 *Effects of Ion Irradiation on* $Zr_{52.5}Cu_{17.9}Ni_{14.6}Al_{10}Ti_5$ *(BAM-11) Bulk Metallic Glass, Intermetallics* **53** 62–6
[15] Luo W, Yang B and Chen G 2011 Effect of Ar^+ ion irradiation on the microstructure and properties of Zr-Cu-Fe-Al bulk metallic glass *Scr. Mater.* **64** 625–8
[16] Li F J, Xing J S, Zhao Z Q and Wei B C 2016 Damage characteristics of Zr-based metallic glasses under helium ions irradiation *Materials Science Forum* (Switzerland: Trans Tech Publ) vol 849, 22–7
[17] Wang B, Mei X, Zhang H, Hou W, Wang Y, Wang Z and Dong C 2014 Resistance to He^{2+} induced irradiation damage in metallic glass $Zr_{64}Cu_{17.8}Ni_{10.7}Al_{7.5}$ *J. Nucl. Mater.* **444** 342–8
[18] Nagase T, Hosokawa T and Umakoshi Y 2006 Solid State Amorphization and Crystallization in $Zr_{66.7}Pd_{33.3}$ Metallic Glass *Intermetallics* **14** 1027–32
[19] Nagase T, Nakamura M and Umakoshi Y 2007 Electron irradiation induced nano-crystallization in $Zr_{66.7}Ni_{33.3}$ amorphous alloy and $Zr_{60}Al_{15}Ni_{25}$ metallic glass *Intermetallics* **15** 211–24
[20] Umakoshi Y, Nagase T and Hosokawa T 2007 Electron irradiation induced crystallization Behavior in $Zr_{66.7}M_{33.3}$ (M= Cu, Ni, Pd) metallic glasses *Materials Transactions* **48** 1644–50
[21] Chen H, Yan L, Liu R, Tang M, Wang G, Huang H, Hai Y and Zhou X 2014 Anisotropic nanocrystallization of a Zr-based metallic glass induced by Xe ion irradiation *Intermetallics* **52** 15–9

[22] Chen H, Cao G, Liu R, Wang G, Yan L and Zhou X 2015 Ion irradiation induced element-enriched and depleted nanostructures in Zr-Al-Cu-Ni metallic glass *J. Appl. Phys.* **118** 035308
[23] Iqbal M, Akhter J, Hu Z, Zhang H, Qayyum A and Sun W 2007 Mechanical properties and ion irradiation of bulk amorphous $Zr_{55}Cu_{30}Al_{10}Ni_5$ alloy *J. Non-Cryst. Solids* **353** 2452–8
[24] Nagase T, Sanda T, Nino A, Qin W, Yasuda H, Mori H, Umakoshi Y and Szpunar J A 2012 MeV electron irradiation induced crystallization in metallic glasses: Atomic structure, crystallization mechanism and stability of an amorphous phase under the irradiation *J. Non-Cryst. Solids* **358** 502–18
[25] Brechtl J, Agarwal S, Crespillo M, Yang T, Bei H and Zinkle S 2019 Evolution of the microstructural and mechanical properties of BAM-11 bulk metallic glass during ion irradiation and annealing *J. Nucl. Mater.* **523** 299–309
[26] Liu T, Guo W, Crespillo M L, Jin K, Zhang Y, Bei H and Gao Y 2020 Indirectly probing the structural change in ion-irradiated Zr-Based metallic glasses from small scale mechanical tests *Intermetallics* **121** 106794
[27] Hori F, Onodera N, Fukumoto Y, Ishii A, Iwase A, Kawasuso A, Yabuuchi A, Maekawa M and Yokoyama Y 2011 A study of defects in electron-and ion-irradiated ZrCuAl bulk glassy alloy using positron annihilation techniques *12th International Workshop on Slow Positron Beam Techniques (SLOPOS12)* vol 262 IOP Publishing *J. Phys. Conf. Ser.* 012025
[28] Bian X, Wang G, Chen H, Yan L, Wang J, Wang Q, Hu P, Ren J, Chan K C, Zheng N *et al* 2016 Manipulation of free volumes in a metallic glass through Xe-ion irradiation *Acta Mater.* **106** 66–77
[29] Chen H, Hai Y, Liu R, Lei Q, Ye L, Xu J, Wang G, Yin W, Yan L and Zhou X 2019 The microstructure and mechanical properties of He^+ ion irradiated $Zr_{55}Cu_{30}Al_{10}Ni_5$ bulk metallic glass *Intermetallics* **104** 52–8
[30] Sun K, Wang G, Wang Y, Chen H, Yan L, Pauly S, Wu Y, Weber H, Wang Q, Huang B *et al* 2020 Structural rejuvenation and relaxation of a metallic glass induced by ion irradiation *Scr. Mater.* **180** 34–9
[31] Qiu Y, Xu C, Fu E, Wang P, Du J, Hu Z, Yan X, Cao X, Wang Y and Shao L 2018 Mechanisms for the free volume tuning the mechanical properties of metallic glass through ion irradiation *Intermetallics* **101** 173–8
[32] Frahm R 1983 Crystallization behaviour of amorphous nickel-zirconium alloys *J. Non-Cryst. Solids* **56** 255–60
[33] Buschow K and Beekmans N 1979 Thermal stability and electronic properties of amorphous Zr-Co and Zr-Ni alloys *Physical Review B* **19** 3843
[34] Yang L, Yin S, Wang X, Cao Q, Jiang J, Saksl K and Franz H 2007 Atomic structure in $Zr_{70}Ni_{30}$ metallic glass *J. Appl. Phys.* **102** 083512
[35] Tyagi A, Nandedkar R and Krishan K 1983 Effect of 100 keV helium ion bombardment on surface topography and microstructure of $Ni_{33}Zr_{67}$ glass *J. Nucl. Mater.* **114** 181–9
[36] Tyagi A and Nandedkar R 1985 Helium irradiation of Ni-(Zr or Nb) metallic glasses: Blistering, flaking and bubble formation *J. Nucl. Mater.* **132** 62–9
[37] Toulemonde M, Assmann W, Dufour C, Meftah A, Studer F and Trautmann C 2006 Experimental phenomena and thermal spike model description of ion tracks in amorphisable inorganic insulators *Mat. Fys. Medd* **52** 263–92 (http://publ.royalacademy.dk/books/163/1016?lang=da)
[38] Ghidelli M, Gravier S, Blandin J J, Pardoen T, Raskin J P and Mompiou F 2014 Compositional-induced structural change in Zr_xNi_{100-x} thin film metallic glasses *J. Alloys Compd.* **615** S348–51
[39] Ziegler J F, Ziegler M D and Biersack J P 2010 SRIM-The stopping and range of ions in matter (2010) *Nucl. Instrum. Methods Phys. Res., Sect. B* **268** 1818–23
[40] Hengstler-Eger R, Baldo P, Beck L, Dorner J, Ertl K, Hoffmann P, Hugenschmidt C, Kirk M, Petry W, Pikart P *et al* 2012 Heavy ion irradiation induced dislocation loops in AREVA's M5® alloy *J. Nucl. Mater.* **423** 170–82
[41] Mwema F M, Akinlabi E T and Oladijo O P 2019 *The use of power spectrum density for surface characterization of thin films (Wiley Online Library) chap* **9** 379–411
[42] Horcas I, Fernández R, Gomez-Rodriguez J, Colchero J, Gómez-Herrero J and Baro A 2007 WSXM: a software for scanning probe microscopy and a tool for nanotechnology *Rev. Sci. Instrum.* **78** 013705
[43] Oliver W C and Pharr G M 1992 An improved technique for determining hardness and elastic modulus using load and displacement sensing indentation experiments *J. Mater. Res.* **7** 1564–83
[44] Yang Y, Zeng J, Volland A, Blandin J, Gravier S and Liu C T 2012 Fractal growth of the dense-packing phase in annealed metallic glass imaged by high-resolution atomic force microscopy *Acta Mater.* **60** 5260–72
[45] Ghidelli M, Volland A, Blandin J J, Pardoen T, Raskin J P, Mompiou F, Djemia P and Gravier S 2014 Exploring the mechanical size effects in $Zr_{65}Ni_{35}$ thin film metallic glasses *J. Alloys Compd.* **615** S90–2
[46] Ghidelli M, Gravier S, Blandin J J, Raskin J P, Lani F and Pardoen T 2014 Size-dependent failure mechanisms in ZrNi thin metallic glass films *Scr. Mater.* **89** 9–12
[47] Volland A 2012 Etude des effets d'échelle sur le comportement mécanique de film mince en verre métallique *Ph.D. thesis* Université de Grenoble (https://theses.hal.science/tel-00872887/file/25976_VOLLAND_2012_archivage1.pdf)
[48] Alshamsi A S and AlBlooshi A 2019 Effect of surface roughness on the corrosion behavior of pure iron in acidic solutions *Int. J. Electrochem. Sci* **14** 5794–812
[49] Evgeny B, Hughes T and Eskin D 2016 Effect of surface roughness on corrosion behaviour of low carbon steel in inhibited 4 M hydrochloric acid under laminar and turbulent flow conditions *Corros. Sci.* **103** 196–205
[50] Leban M B, Mikyška Č, Kosec T, Markoli B and Kovač J 2014 The effect of surface roughness on the corrosion properties of type AISI 304 stainless steel in diluted NaCl and urban rain solution *J. Mater. Eng. Perform.* **23** 1695–702
[51] Thomas S, Thomas H, Avasthi D, Tripathi A, Ramanujan R and Anantharaman M 2009 Swift heavy ion induced surface modification for tailoring coercivity in Fe-Ni based amorphous thin films *J. Appl. Phys.* **105** 033910
[52] Thomas H, Thomas S, Ramanujan R V, Avasthi D, Al-Omari I, Al-Harthi S and Anantharaman M 2012 Swift heavy ion induced surface and microstructural evolution in metallic glass thin films *Nucl. Instrum. Methods Phys. Res., Sect. B* **287** 85–90
[53] Huang Y, Zhou B, Fan H, Wang Y, Wang D, Sun J and Shen J 2014 Effect of ion irradiation in an $Al_{90}Fe_2Ce_8$ metallic glass *Materials & Design (1980-2015)* **62** 133–6
[54] Mayr S and Averback R 2001 Surface smoothing of rough amorphous films by irradiation-induced viscous flow *Phys. Rev. Lett.* **87** 196106
[55] Hou W, Mei X, Zhang X, Wang Y, Qiang J, Sun J and Wang Y 2016 Resistance to He^{2+} irradiation damage in metallic glass $Ta_{38}Ni_{62}$ *Appl. Surf. Sci.* **383** 106–12
[56] Zhang H, Mei X, Zhang X, Li X, Wang Y, Sun J and Wang Y 2016 H+-induced irradiation damage resistance in Fe-and Ni-based metallic glass *Nucl. Instrum. Methods Phys. Res., Sect. B* **375** 79–86
[57] Hysen T, Geetha P, Al-Harthi S, Al-Omari I, Lisha R, Ramanujan R, Sakthikumar D, Avasthi D and Anantharaman M 2014 Effect of 100 MeV Ag^{+7} ion irradiation on the bulk and surface magnetic properties of Co-Fe-Si thin films *J. Magn. Magn. Mater.* **372** 224–32

[58] Tong W M and Williams R S 1994 Kinetics of surface growth: phenomenology, scaling, and mechanisms of smoothening and roughening *Annu. Rev. Phys. Chem.* **45** 401–38
[59] Herring C 1950 Effect of change of scale on sintering phenomena *J. Appl. Phys.* **21** 301–3
[60] Pookat G, Hysen T, Al-Harthi S, Al-Omari I, Lisha R, Avasthi D and Anantharaman M 2013 Magnetic and topographical modifications of amorphous Co-Fe thin films induced by high energy Ag $^{7\cdot}$ ion irradiation *Nucl. Instrum. Methods Phys. Res., Sect. B* **310** 81–6
[61] Mayr S, Ashkenazy Y, Albe K and Averback R 2003 Mechanisms of radiation-induced viscous flow: Role of point defects *Phys. Rev. Lett.* **90** 055505
[62] Brechtl J, Wang H, Kumar N, Yang T, Lin Y R, Bei H, Neuefeind J, Dmowski W and Zinkle S J 2019 Investigation of the thermal and neutron irradiation response of BAM-11 bulk metallic glass *J. Nucl. Mater.* **526** 151771
[63] Raghavan R, Kombaiah B, Döbeli M, Erni R, Ramamurty U and Michler J 2012 Nanoindentation response of an ion irradiated Zr-based bulk metallic glass *Materials Science and Engineering: A* **532** 407–13
[64] Sadeghilaridjani M, Ayyagari A, Muskeri S, Hasannaeimi V, Jiang J and Mukherjee S 2020 Small-scale mechanical behavior of ion-irradiated bulk metallic glass *JOM* **72** 123–9
[65] Brechtl J, Crespillo M L, Agarwal S, Bei H and Zinkle S J 2020 Effects of irradiation spectrum on the microstructural and mechanical properties of bulk metallic glasses *J. Nucl. Mater.* **533** 152084
[66] Onodera N, Ishii A, Fukumoto Y, Iwase A, Yokoyama Y and Hori F 2012 Local structure and hardness change of $Zr_{50}Cu_{40}Al_{10}$ bulk glassy alloy after heavy ion irradiation *Nucl. Instrum. Methods Phys. Res., Sect. B* **282** 1–3
[67] Byun T and Farrell K 2004 Irradiation hardening behavior of polycrystalline metals after low temperature irradiation *J. Nucl. Mater.* **326** 86–96
[68] Huang Y, Fan H, Zhou X, Xue P, Ning Z, Daisenberger D, Sun J and Shen J 2015 Structure and mechanical property modification of a Ti-based metallic glass by ion irradiation *Scr. Mater.* **103** 41–4
[69] Liang Y, Du J, Xu C, Wang P, Hu Z, Qiu Y, Wang P and Fu E 2019 Roles of ion irradiation and thermal annealing in inducing crystallization in metallic glass *Intermetallics* **114** 106608
[70] Chen H 1983 Structural relaxation in metallic glasses *Amorphous metallic alloys* (USA: Butterworth-Heinemann) 169–86
[71] Suryanarayana C and Inoue A 2012 Metallic Glasses *in Ullmann's Encyclopedia of Industrial Chemistry* (Germany: Wiley-VCH Verlag GmbH:Weinheim) (https://doi.org/10.1002/14356007.a16_335.pub2)
[72] Kartouzian A 2013 Cluster-assembled metallic glasses *Nanoscale Res. Lett.* **8** 1–4
[73] WH J, FX L and Choo H 2007 Effect of structural relaxation on mechanical behavior of a Zr-based bulk-metallic glass *Materials Transactions* **48** 1781–4
[74] Leyland A and Matthews A 2000 On the significance of the H/E ratio in wear control: a nanocomposite coating approach to optimised tribological behaviour *Wear* **246** 1–11
[75] Shao L, Gorman B P, Aitkaliyeva A, David Theodore N and Xie G 2012 Nanometer-scale tunnel formation in metallic glass by helium ion irradiation *Appl. Phys. Lett.* **101** 041901
[76] Yiu P, Diyatmika W, Bönninghoff N, Lu Y C, Lai B Z and Chu J P 2020 Thin film metallic glasses: Properties, applications and future *J. Appl. Phys.* **127** 030901
[77] Lee G C, Noh H, Yeom H, Jo H, Kim T K, Kim M, Sridharan K and Park H S 2019 Zirconium-silicide coating on zircaloy-4 substrate for accident tolerance: Effects on oxidation resistance and boiling *Ann. Nucl. Energy* **126** 350–8
[78] Tunes M A, Vishnyakov V M, Camara O, Greaves G, Edmondson P D, Zhang Y and Donnelly S E 2019 A candidate accident tolerant fuel system based on a highly concentrated alloy thin film *Materials Today Energy* **12** 356–62
[79] Waligorski M, Hamm R and Katz R 1986 The radial distribution of dose around the path of a heavy ion in liquid water *Int. J. Radiat. Appl. Instrum. Part D* **11** 309–19
[80] Ichitsubo T, Matsubara E, Saida J and Chen H S 2005 Local structure and glass transition in Zr-based binary amorphous alloys *Materials Transactions* **46** 2282–6
[81] Jana A, Sridar S, Fries S G, Hammerschmidt T and Kumar K H 2020 Thermodynamic modelling of the Ni-Zr system *Intermetallics* **116** 106640
[82] Yamasaki M, Kagao S, Kawamura Y and Yoshimura K 2004 Thermal diffusivity and conductivity of supercooled liquid in $Zr_{41}Ti_{14}Cu_{12}Ni_{10}Be_{23}$ metallic glass *Appl. Phys. Lett.* **84** 4653–5
[83] Inoue A, Matsuzaki K, Masumoto T and Chen H 1986 Superconducting and electrical properties of amorphous zirconium-transition metal binary alloys *J. Mater. Sci.* **21** 1258–68
[84] Myers M, Fu E, Myers M, Wang H, Xie G, Wang X, Chu W and Shao L 2010 An experimental and modeling study on the role of damage cascade formation in nanocrystalization of ion-irradiated $Ni_{52.5}Nb_{10}Zr_{15}Ti_{15}Pt_{7.5}$ metallic glass *Scr. Mater.* **63** 1045–8